Journal of Materials Chemistry C

Accepted Manuscript

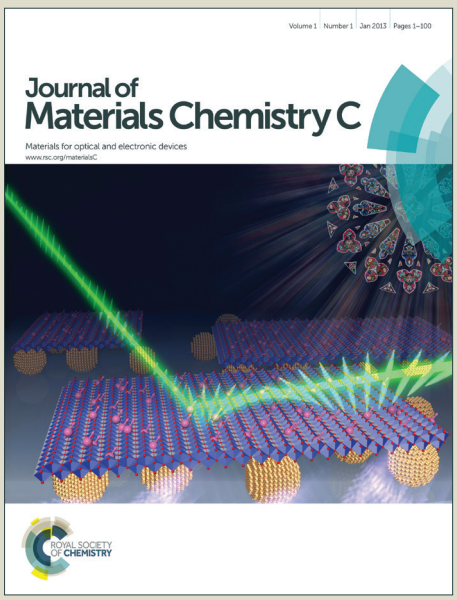

ROYAL SOCIETY OF CHEMISTRY

www.rsc.org/materialsC

Journal Name

RSCPublishing

ARTICLE

Organic nanowire waveguide exciton-polariton sub-microlaser and its photonic application

Cite this: DOI: 10.1039/xoxxoooooox

Qing Liao[a,b*], Zhenzhen Xu[b,c], Xiaolan Zhong[d], Wei Dang[e], Qiang Shi[b], Chao Zhang[d], Yuxiang Weng[e], Zhiyuan Li[d] and Hongbing Fu[a,b*]

Received ooth January 2012,
Accepted ooth January 2012

DOI: 10.1039/xoxxoooooox

www.rsc.org/

Development of nanoscale optical components has been an active topic in nanophotonics, with potential for use in high-speed data highways on electronic chips. Organic semiconductors are low-cost advanced materials, exhibiting ease of processing, along with chemically tunable electronic and optical properties. Moreover, the large binding energy and oscillator strength of Frenkel excitons make polaritons in organic semiconductors highly stable at room temperature. Here, we demonstrate a waveguide exciton-polariton (WGEP) sub-microlaser from a built-in Fabry-Pérot (FP) cavity based on self-assembled organic nanowires (ONWs) of 1,4-chloride-2,5-di[4'-(methlthio)styryl-benzene (CDSB). The strong light-matter coupling results in strong optical confinement, enabling ONWs to guide and steer WGEP laser light at the wavelength scale. An optical router was realized using a dendritic structure as a result of efficient polariton waveguiding and photoluminescence (PL) anisotropy of ONWs, opening a new route to future photonic circuits.

Introduction

In recent years the ever-increasing demands on high-speed optical communication and data processing had inspired great efforts for development of nanophotonics[1-8]. Based on semiconductor nanowires, a myriad of nanoscale on-chip optical components had been realized, including lasers, waveguide interconnectors, routers, and all-optic switches[1-7]. Organic semiconductors are very promising advanced materials for nanophotonics due to their low-cost, their ease of processing, and their chemically tunable electronic and optical properties[9,10]. Optically pumped organic lasers had been reported in a variety of resonator geometries, such as micro-ring, distributed feedback (DFB), and photonic bandgap structures[11]. The active medium in these devices generally consists of an amorphous or polycrystalline film, in which unavoidable structural disorder and grain boundaries limit the device performance. Most recently, single-crystalline ONWs self-assembled from π-conjugated semiconductors has shown superior charge mobility to amorphous or polycrystalline films[12]. This, combined with recently observed optical waveguiding and lasing action[13, 14], make ONWs very attractive candidates for future photonic circuits.

Strong coupling of confined photons with Wannier-Mott excitons in semiconductor quantum microcavities generates half-light half-matter exciton polaritons (EPs)[15], which have enabled observations of Bose-Einstein condensation[16], low-threshold polariton lasing[17] and bright polariton solitons[18]. As compared with Wannier-Mott excitons in inorganic semiconductors, Frenkel excitons in organic semiconductors possess higher binding energy and larger oscillator strength[19], making EPs highly stable in these materials at room temperature[20-22]. Recently, Forrest and co-workers demonstrated the room-temperature polariton lasing from an organic planar microcavity, in which a melt-grown single-crystalline ultrathin layer of anthracene is placed at the antinode of a λ/2-microcavity made by two DBRs[21]. This planar microcavity confines the photon field in the *z*-direction, while the in-plane wave-vector $k_{//}$ changes continuously. As a result, EPs are two-dimensionally confined in planar microcavities, with the upper and the lower polariton branches (UPB and LPB) anti-crossing in the $k_{//}$ space. Under lasing conditions, increase in LPB population at $k_{//} = 0$ had been observed due to non-equilibrium condensation of EPs, leading to a threshold lower than that calculated for conventional photon lasing[21]. Different from the planar microcavity, faceted ONWs confine photons one dimensionally with two end-faces as two reflectors forming a FP cavity along its length, in which waveguide modes of confined photons ($k_{//}$ = fixed values, k_z is quantized) can couple with excitons generating waveguide exciton-polaritons (WGEPs). Takazawa and co-workers reported that WGEPs exhibit remarkable propagation properties in J-aggregate organic nanofibers[22]. Most recently, two-photon pumped lasing in ONW WGEP microresonators was observed at liquid-nitrogen temperature of 77 K, with the photonic part rather than the excitonic part of WGEPs playing the major in the lasing

action[23]. In this letter, we demonstrate a room-temperature WGEP sub-microlaser from a built-in FP cavity based on self-assembled ONWs of CDSB. We found that strong light-matter coupling leads to a significantly slowed group velocity and therefore a high group refractive index, allowing ONWs to guide and steer WGEP laser light at the wavelength scale. The strong WGEP optical confinement and PL anisotropy of highly ordered ONWs make them attractive candidates for future photonic circuits.

Results and discussion

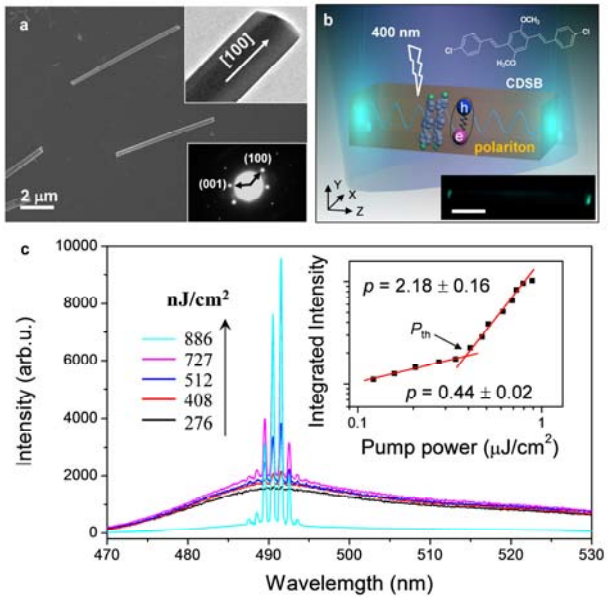

Figure 1. (a) SEM image of the as-prepared ONWs. Insets show the corresponding TEM (upper) and SAED (lower) images. (b) A schematic illustration of the formation, propagation and emission of WGEPs in CDSB ONW microcavity. The insets are the molecular structure of CDSB (upper) and micro-area PL images of one single ONW (lower). (c) PL spectra of an ONW with L = 10.4 μm as a function of pump laser power at 400 nm. The inset shows the power-dependence profile of integrated PL intensities of 0–1 peak. The lasing threshold is identified as the intersection between the sublinear and superlinear regions.

In our experiment, regularly shaped ONWs of CDSB were prepared by a solution self-assembly method[13], upon injection of 100 μL of a stock solution of CDSB (5 mM) in tetrahydrofuran into 2.0 mL of hexane under stirring. Scanning and transmission electron microscopy (SEM and TEM) results (Figure 1a) confirm that these nanowires are well faceted with a rectangular cross-section [width (W) = 1–2 μm; height (H) = 0.5–0.8 × W] uniformly distributed along the entire length (L) of several to several tens of micrometers. The selected area electron diffraction (SAED) and X-ray diffraction (XRD) analyses (inset of Figure 1a and Figure S1) further indicate that our rectangular ONWs are single crystals and can be indexed to monoclinic CDSB crystal, with cell parameters of a = 9.6685 (19) Å, b = 22.865 (5) Å, c = 9.6903 (19) Å, α = γ = 90°, and β = 112.41° (Figure S1). The spots (Inset of Figure 1a) are due to (100) and (001) Bragg reflections with lattice spacing (d) values of $d_{(100)}$ = 9.66 Å and $d_{(001)}$ = 9.69 Å, respectively. According to the SAED pattern suggests that the preferential growth orientation of ONWs is along [100] direction and in which CDSB molecules stack at a tilting angle of 75.3° along the nanowire Z-direction (Figure 1b).

To investigate the lasing effect, we studied single ONW using a home-made optical microscope equipped with a 50× 0.9 NA objective. The second harmonic (λ = 400 nm, pulse width 150 fs) of a 1 kHz Ti:sapphire regenerative amplifier was focused to a 50-μm-diameter spot to excite the selected single ONW wholly. The micro-area PL image shows that rectangular ONWs exhibit a strong optical confinement effect: the ONWs are able to absorb the excitation light and the PL propagates along the 1D direction, leading to bright tips when the PL exits the ONWs (Figure 1b)[23, 24]. In our setup (Figure 1b and Scheme S2), the spectrum of PL leaked at the ONW end was collected underneath using another 3D-movable objective coupled to an optical fiber and detected using a liquid-nitrogen cooled charge-coupled device (CCD).

Figure 1c depicts the guided PL spectra of an ONW with L = 10.4 μm, as a function of pump laser power varied using a series of metallic neutral density filters. At low pump density of P = 276 nJ/cm^2, the PL spectrum displays broad 0–1 and 0–2 spontaneous emission bands at 490 and 525 nm, respectively. And the 0–0 emission band at 465 nm, which is well resolved in the PL spectrum of CDSB powder (Figure 3a and S2), is almost undetectable in ONWs probably owing to the self-absorption effect occurring during the PL waveguiding process[25]. Upon increasing the pump density from P = 276 nJ/cm^2 to P = 727 nJ/cm^2, strong laser emission develops as a set of sharp peaks on the top of 0–1 transition, indicating the resonant cavity modes. With further increasing of pump density, these modes become dominant in the PL spectra, as indicated by the cyan line in Figure 1b recorded at P = 886 nJ/cm^2. And the individual cavity mode presents a line-width as narrow as 0.6 nm. Meanwhile, the full width at half maximum (FWHM) of the 0–1 peak-contour dramatically decreases from 28 nm at P = 276 nJ/cm^2 to 6 nm at P = 886 nJ/cm^2. The inset of Figure 1c shows the integrated intensities of 0–1 peak as a function of pump density, showing clearly an intersection point at P_{th} = 384 nJ/cm^2 defined as the lasing threshold. And the intensity dependence of 0–1 peak can be fitted to a power law of x^p with p = 0.44 ± 0.02 below threshold and p = 2.18 ± 0.16 above threshold, indicating a transition from sublinear regime that is dominated by bimolecular quenching to a superlinear regime[13, 21]. In sharp contrast, the 0–2 band remains in the sublinear regime both below and above threshold. Furthermore, we found that the laser emission is linearly polarized and follows a function of $\sin^2(\theta)$ as expected for TE polarization (Figure S3), where θ is the angle between the X-direction in Figure 1a and the polarizer (Scheme S3).

To avoid the saturation of CCD camera, we usually used a shorter CCD-exposure time (100 ms) to collect the spectra during the lasing experiment as shown in Figure 1b. The poor signal-to-noise ratio due to the fluctuation of excitation laser degrades the contrast of spectral fringes below threshold. Upon extending the CCD-exposure time (500 ms), we could observe cavity resonances also below threshold over the entire spectral range covering both the 0-1 and 0-2 transition. Figure 2b

depicts that the lasing modes of the 10.4-μm-long ONW observed above threshold (red line) are in good agreement with those FP modes observed below threshold (black line). This suggests that similar cavity operates below and above threshold. In order to understand the influence of ONW sizes on cavity effect, we investigated hundreds of ONWs with L = 3–20 μm: i) 90% of them presents thresholds (50–500 nJ/cm^2) for superlinear output, spectral narrowing, and periodic intensity modulation; ii) about 30% of them also exhibit cavity resonances below threshold with a pattern similar to that observed above threshold. Figure 2a and c give two examples of ONW WGEP lasers with L = 7.9 and 20.1 μm, respectively. For a FP cavity of length L (Supporting Information), the mode spacing ($\Delta\lambda$) at λ is given by $\Delta\lambda = (\lambda^2/2L)[n\text{-}\lambda(dn/d\lambda)]^{-1}$, where n is the phase refractive index and $dn/d\lambda$ the dispersion relation[14]. Figure 2d plots the mode spacing of $\Delta\lambda$ at λ = 490 (black squares) and 525 nm (red circles) versus 1/L of ONWs. As one can see, both can be fitted linearly, confirming that the pair of optically flat end faces of an ONW can function as two reflectors, forming an FP microcavity along its length (middle image in Figure 1a). The group refractive index of $[n\text{-}\lambda(dn/d\lambda)]$ for light that travels at least a round trip was determined according to $[n\text{-}\lambda(dn/d\lambda)] = (\lambda^2/2\Delta\lambda L)$, based on FP resonant modes of individual single ONWs with different lengths. Figure 2e presents the dispersion curve of group refractive index at different wavelengths, calculated from the data shown in Figure 2a-c and S5. The value of $[n\text{-}\lambda(dn/d\lambda)]$ is constant around 3.8 for λ > 520 nm, and then increases rapidly with decreasing the wavelength. And $[n\text{-}\lambda(dn/d\lambda)]$ = ~11 is obtained at 490 nm, much larger than reported values (ca. 3~4) for organic FP cavity lasers[14, 23-26]. Note that similar results, i.e., the enhanced group index, had also been reported for J-aggregate organic nanofibers and ZnO nanowires, and were ascribed to strong light-matter coupling that creates WGEPs propagating along the 1D nanostructure[22].

In conventional planar microcavities, the energy~in-plane-wavevector (E~$k_{//}$) dispersion can be determined by angle-resolved reflection or PL measurements to characterize the exciton-photon coupling[15-17, 20, 21]. This, however, are not applicable for our ONWs, in which the value of $k_{//}$ is factually a fixed value due to the limitation of section dimensions. By extracting the energy positions of FP cavity resonances, for example, those presented in the black spectrum in Figure 2a-c, we could reconstruct the energy~wavevector (E~k_z) dispersion of propagating modes by placing the interference peaks at integer multiples of π/L in the space of k_z[27]. The obtained E~k_z dispersion of the propagating modes exhibits significant curvature (triangles in Figure 3b). We simulated this WGEP dispersion using a coupled oscillator model based on equation (1) (refs. 20 and 21),

$$\begin{pmatrix} E_{ph}-E & V \\ V & E_{ex}-E \end{pmatrix}\begin{pmatrix} \alpha \\ \beta \end{pmatrix} = 0 \qquad (1)$$

Here E_{ph} and E_{ex} are the energies of the uncoupled cavity photon and the bare exciton, respectively, and V represents the coupling potential between them. E are the new eigenvalues of

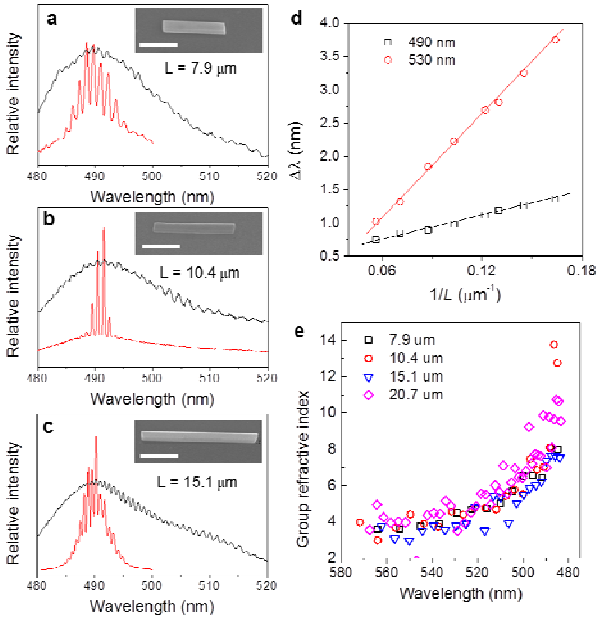

Figure 2. (a)-(c) High-resolution PL spectra of below (black) and above threshold (red) for ONWs with L = 7.9, 10.4 and 15.1 μm, respectively. Insets show high-magnification SEM images of the corresponding single ONW. The scale bar is 5 μm. (d) Plot of the mode spacing Δλ at 490 nm (black square) and 530 nm (red circle) as a function of 1/L. (e) The relationship of group refractive index (n-$\lambda dn/d\lambda$) vs. wavelength, determined from ONWs with L = 7.9, 10.4, 15.1 and 20.7 μm, respectively.

the coupled system of WGEPs with $|\alpha|^2$ and $|\beta|^2$ of the mixing coefficients of the cavity photon and the exciton, respectively. Good fits were obtained based on eq. (1) with E_{ex} = 2.72~2.87 eV, which corresponds to |10> excitons as determined from the absorption spectra (Figure 3a), yielding V = 0.355~0.617 eV (Table S1). Figure 3b shows an example for E_{ex} = 2.80 eV. Anti-crossing is clearly observed between upper and lower polariton branches (UPB and LPB) with a separation of Rabi splitting energy, $\Omega = 2V$ = 1.0 eV, orders of magnitude larger than that in semiconductor microcavities[15-17]. Figure 3c depicts the mixing coefficients of $|\alpha|^2$ and $|\beta|^2$ extracted from the coupled oscillator model plotted versus k_z for LPB. It is apparent that the excitonic component is dominant with $|\beta|^2$ around 0.9 in the spectral range where WGEP lasing takes place (marked by blue circles in Figure 3a). Therefore, it is the matter side of polaritons, rather than the light side, that plays the major role in the observed WGEP lasing action.

In the case of our CDSB ONWs, 400-nm femtosecond laser excitation produces high-energy |1n> excitons (the first and second number denotes the electronic and vibrational states, respectively), which then undergo fast vibrational relaxation giving rise to a reservoir of lowest-energy |10> excitons (inset of Figure 3a). Spontaneous emission occurs from the relaxed |10> state to vibronic sublevels of the ground state. In organic semiconductors, the vibrationally excited ground state, i.e., |01> state, is unoccupied in thermal equilibrium, providing a four-level diagram that facilitates the stimulated transition from |10> to |01> states (inset of Figure 3a). Recently, Mazza and La Rocca theothretically demonstrated that direct pumping of

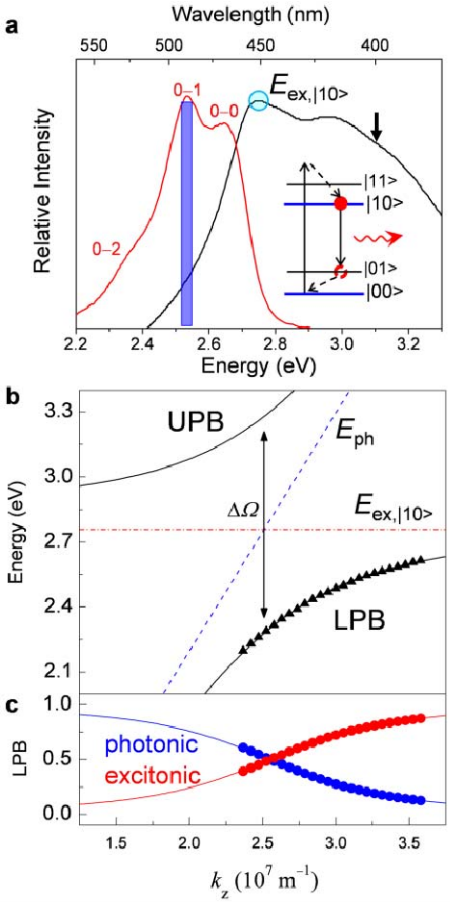

Figure 3. (a) Diffused reflectance absorption (black) and spontaneous PL (blue) spectra of a 110-nm-thick film of CDSB. **Inset:** Energy level diagram of CDSB ONWs. (b) E~k_z dispersion relation of WGEPs (triangle), obtained by placing those FP interference peaks extracted from the balck spectrum in **Figure 2b** at integer multiples of π/L in the space of k_z. The black line represents a fit following the coupled harmonic oscillator Hamitonian eq. (1) using E_{ex} = 2.80 eV, yield a Rabi splitting of $\Omega = 2V = 1.0$ eV. The red- and blue-dashed lines obey the dispersions of uncoupled exciton and light, respectively. (c) Photonic and excitonic branch content for lower polariton branch.

exciton reservoir into LPB through PL processes can selectively populate LPB states, which have an energy separation from the exciton reservoir equal to quanta of molecular vibrations. To examine the scattering mechanism from the reservoir of |10> exctions to LPB, we systematically investigated the PL lifetimes of a 10.4-μm-long ONW at different pump densities using a streak camera, as shown in Figure 4a. At very low excitation density (P = 0.04 P_{th}), the emission follows single exponential decay with a time constant of τ_{ONW} = 1.00 ± 0.06 ns. Based on the measurement of PL quantum yield of DASB ONWs, Φ_{ONW} = 0.92 ± 0.03, the radiative and nonradiative decay rates of exciton reservoir were determined to be k_{nr} = 0.08 ns^{-1} << k_r = 0.92 ns^{-1}, according to $k_r = \Phi/\tau$ and $\tau = (k_r + k_{nr})^{-1}$. This suggests that scattering of exciton reservoir into LPB via nonradiative emission of vibrational phonons, i.e., k_{nr}, is negligible in our system. Upon increasing the pump intensity to P = 0.25 P_{th}, PL of CDSB ONWs decays bi-exponentially with the fast component ascribed to the presence of bimolecular quenching. Above threshold (P = 1.55 P_{th}), the emission decay time always collapses to < 20 ps (limited by the resolution of the streak camera). By using a planar λ/2-microcavity, Forrest and co-workers observed an accumulation of LPB at $k_{//}$ = 0 under lasing conditions due to non-equilibrium condensation of EPs. In our system, this is, however, unclear yet. And the fast decay time < 20 ps observed in ONW WGEP laser indicates a stimulated radiative scattering from the exciton reservoir to LPB.

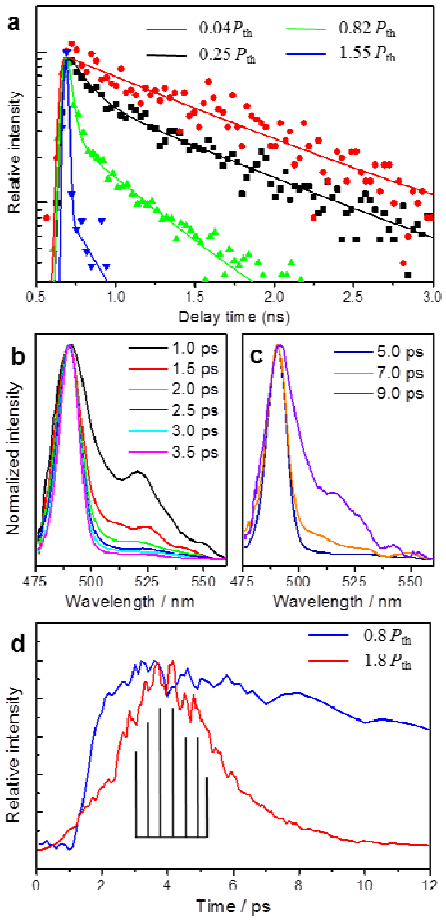

Figure 4. (a) Typical PL decay profiles of a 10-μm-long ONW monitored at 490 nm using a streak camera. The 10-μm-long ONW was fully excited with a 400-nm, 150-fs laser spot around 20 μm in diameter. (b) and (c) Time-resolved emission spectra recorded using NOPA method at different delay times after excitation with femtosecond laser at 400 nm. (d) Typical PL decay profiles at 400 nm below (blue) and above threshold (red) recorded by using NOPA method.

To further understand the lasing dynamics, femtosecond time-resolved transient fluorescence was measured based on non-collinear optical parametric amplification (NOPA) technique[28]. Figure 4b and c show the spectral evolution of polariton lasing as a function of delay time. The one at the early stage with a delay time 1.0 ps exhibits characteristics of amplified spontaneous emission (ASE). With increasing the delay time, the 0–1 peak develops rapidly and becomes narrower, indicating that the cavity feedback concentrates the LPB population into those cavity resonant modes around the gain maximum in the vicinity of 490 nm. After the delay time exceeds 7 ps (Figure 4c), ASE characteristics registers again,

suggesting that the short cavity photon lifetime determines the polariton decay rate in our system.

Figure 4d plots the normalized PL intensities at 490 nm as a function of delay time below and above threshold. The one below threshold (blue line) decays exponentially with a time constant similar to the fast component measured using the streak camera as shown in Figure 4a. In sharp contrast, the one above threshold (red line) presents as a Gaussian profile with a FWHM of ca. 3.2 ps, which is factually the pulse temporal profile of ONW polariton laser. As compared with the one below threshold, the one above threshold exhibits a slower rising edge and a faster lifetime, strongly supporting the lasing process. Meanwhile, the PL dynamic behaviors at 525 nm are found to be the same below and above threshold (Figure S6), and are almost identical to that measured at 490 nm below threshold (blue line in Figure 4d). Furthermore, we found that the PL decay profile at 490 nm above threshold (red line in Figure 4d) exhibits periodic oscillations after the delay time > 2.5 ps, probably as a result of back and forth reflections of propagation light between two ONW ends. According to the oscillating period, ~ 400 fs, which corresponds to a single trip between two ONW ends along the length of 10 μm, the group velocity of propagation light is determined to be $c/12$ (c: the light speed in vacuum), consistent with the calculated group refractive index of $[n\text{-}\lambda(dn/d\lambda)] = \sim 11$ at 490 nm (Figure 2e). This further verifies our observation of polariton lasing in ONW microcavities.

The numerical calculation based on three-dimensional finite difference time domain (FDTD) method reveals that WGEPs are tightly confined in the center of ONWs (Figure S7). The lateral size of our ONW could allow many types of modes in the cavity. We only considered the lowest order TE mode, based on two facts: i) polarization measurement and ii) this fundamental mode has the highest reflection coefficient on the two end-faces of the ONW cavity. Actually, the optical loss (α) for WGEP propagation along ONWs was measure to be ~ 68 cm^{-1} (Figure S8), far less than that observed for common nanowire photon waveguiding[14, 25]. So threshold gain (g_{th}) is also estimated as high as 433~677 cm^{-1} for ONWs with L = 6~10 μm, according to $g_{th} = \alpha + (1/2L)\ln(R^{-2})$, where R is the reflectivity of ONW end facets (~69.4%; Fresnel equations)[14].

To demonstrate the utility of our ONW WGEP sub-microlasers in the context of photonic circuit, we fabricated an optical router using an ONW dendritic structure (Figure 5a and S8). With one end excited by a focused laser (400-nm and 150-fs) under lasing conditions, locally generated WGEP laser light (black line, Figure 5b) can not only be guided along the rectilinear direction to tip-I (red line), but also be steered over a bending angle of 105° to tip-II (blue line). Remarkably, the output lasing from the two tips are both linearly polarized but along their respective ONW width directions (Figure 5a). And the output polarizations from tip-I and -II exhibit a phase difference of 75° (Figure 5d), equal to the angle between the truck and the branch ONWs (Figure 5a and S9). The coupling efficiency (η) to tip-I or -II can be defined as the ratio between PL intensities recorded at the excitation point and at the tip-I or -II, respectively. Figure 4c reveals that in contrast to η_I, the value of η_{II} is wavelength-dependent and reaches a maximum (~0.25) at 490 nm. This is consistent with FDTD calculations (inset of Figure 5c).

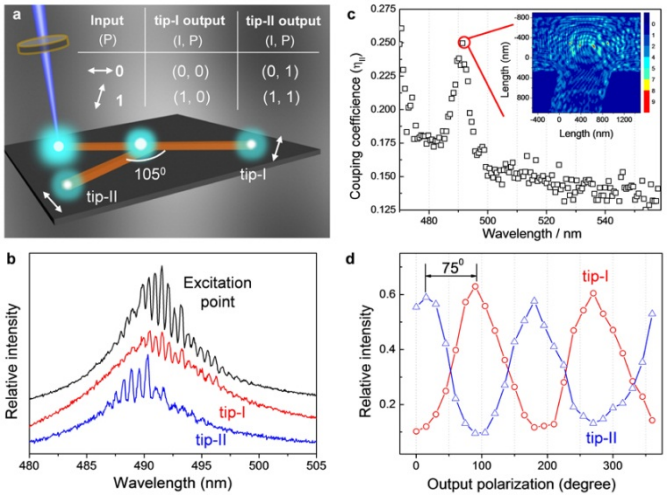

Figure 5. An optical router constructed with an ONW dendritic structure. (a) A schematic illustration of a dendritic structure with one-end excited by focused fs-laser under lasing conditions. The inset shows optical logic gates using the excitation light polarization as inputs and the polarization (P) and intensity (I) of output-lasing emissions at tip-I and -II as outputs. (b) Spatially resolved spectra of WGEP lasing emissions from the regions marked in the (a). (c) The coupling efficiency of WGEP laser light to tip-II (η_{II}) as a function of wavelength. Inset shows the simulated result using the FDTD method for coupling efficiency at 490 nm. (d) Scattering intensity of guided polariton laser light recorded at tip-I (red circle) and tip-II (blue triangle) as a function of polarization angle between the trunk ONW length direction and the polarizer.

Note that the output-lasing intensities at tip-I and -II both can be actively modulated by the excitation light polarization. As the angle (δ) between the polarization of excitation laser and the axis of ONW trunk is adjusted (Figure S8), the output-lasing intensities oscillate between the minimum (I_{min}, as the '0' or 'off' state, $\delta = 0°$) and the maximum (I_{max}, as the '1' or 'on' state, $\delta = 90°$) with an on/off ratio (I_{max}/I_{min}) as large as ~7.0. If the input signal is (0, $\delta = 0°$), the intensity of output light at tip-I is minimally emitting and its polarization is parallel, i.e., (0, 0), while that at tip-II is a minimum and its polarization is perpendicular, i.e., (0, 1). Similarly, when we change input signal to (1, δ = 90°), the (1, 0) and (1, 1) output can be obtained from tip-I and -II, respectively. Thus, the behavior of an optical router was obtained by the utilization of both intensity and polarization as the fundamental features of a photon.

Conclusions

In conclusion, multimode WGEP lasing was observed at room temperature from a built-in optical microcavity based on single-crystalline ONWs. The strong light-matter coupling, manifested by a Rabi splitting energy of ~1 eV, significantly slows down the light group velocity to $c/12$ and therefore results in strong optical confinement in ONW microcavities. The short pulse-width of 3.2 ps observed for our ONW WGEP laser suggests a bosonic final-state stimulated formation of LPB

ensemble, providing a way to decrease the threshold required by achieving electrically pumped organic lasers. We demonstrated an optical router using an ONW dendritic structure as a result of efficient polariton waveguiding and PL polarization anisotropy of output lasing emissions, opening a new route to future photonic circuits.

Acknowledgements

This work was supported by the National Natural Science Foundation of China (Nos. 21073200；21273251；91333111, 20925309, 21190034, 21221002), Beijing Municipal Science & Technology Commission (No. Z131103002813097), the National Basic Research Program of China (973) 2011CB808402, 2013CB933500, and the Chinese Academy of Sciences.

Notes and references

[a] Beijing Key Laboratory for Optical Materials and Photonic Devices, Department of Chemistry, Capital Normal University, Beijing 100048, P. R. China

[b] Beijing National Laboratory for Molecular Science, Institute of Chemistry, Chinese Academy of Sciences, Beijing 100190, P. R. China

[c] The University of Chinese Academy of Sciences, Beijing 100039, P. R. China

[d] Laboratory of Optical Physics, Institute of Physics, Chinese Academy of Science, Beijing 100190, P. R. China

[e] Key laboratory of Soft Matter Physics, Institute of Physics, Chinese Academy of Sciences, Beijing 100190, P. R. China

*E-mail: hongbing.fu@iccas.ac.cn; liaoqing@cnu.edu.cn

† Electronic Supplementary Information (ESI) available: [details of any supplementary information available should be included here]. See DOI: 10.1039/b000000x/

1. R. F. Service, *Science* 2010, **328**, 810-811.
2. M. Law, D. J. Sirbuly, J. C. Johnson, J. Goldberger, R. J. Saykally and P. D. Yang, *Science* 2004, **305**, 1269-1273.
3. H. Wei, Z. Wang, X. Tian, M. Kall and H. Xu, *Nat. Commun.* 2011, **2**, 387-391.
4. B. Piccione, C.-H. Cho, L. K. van Vugt and R. Agarwal, *Nat. Nanotechnol.* 2012, **7**, 640-645.
5. R. Kirchain and L. Kimerling, *Nat. Photon.* 2007, **1**, 303-305.
6. H. J. Caulfield and S. Dolev, *Nat. Photon.* 2010, **4**, 261-263.
7. X. Hu, P. Jiang, C. Ding, H. Yang and Q. Gong, *Nat. Photon.* 2008, **2**, 185-189.
8. R. Yan, D. Gargas and P. Yang, *Nat. Photon.* 2009, **3**, 569-576.
9. M. Pope, C. E. Swenberg and M. Pope, Electronic Processes in Organic Crystals and Polymers, 2nd edn, Oxford Univ. Press: 1999.
10. J. Clark and G. Lanzani, *Nat. Photon.* 2010, **4**, 438-446.
11. I. Samuel and G. Turnbull, *Chem. Rev.* 2007, **107**, 1272-1295.
12. S. Dong, H. Zhang, L. Yang, M. Bai, Y. Yao, H. Chen, L. Gan, Yang, T. H. Jiang, S. Hou, L. Wan and X. Guo, *Adv. Mater.* 2012, **24**, 5576-5580.
13. Z. Xu, Q. Liao, Q. Shi, H. Zhang, J. Yao and H. Fu, *Adv. Mater.* 2012, **24**, OP216-OP220.
14. D. O'Carroll, I. Lieberwirth and G. Redmond, *Nat. Nanotechnol.* 2007, **2**, 180-184.
15. H. M. Gibbs, G. Khitrova and S. W. Koch, *Nat. Photon.* 2011, **5**, 275-282.
16. J. Kasprzak, M. Richard, S. Kundermann, A. Baas, P. Jeambrun, J. M. J. Keeling, F. M. Marchetti, M. H. Szymanska, R. Andre, J. L. Staehli, V. Savona, P. B. Littlewood, B. Deveaud and L. S. Dang, *Nature* 2006, **443**, 409-414.
17. A. Das, J. Heo, M. Jankowski, W. Guo, L. Zhang, H. Deng, and P. Bhattacharya, *Phys. Rev. Lett.* 2011, **107**, 066405.
18. M. Sich, D. N. Krizhanovskii, M. S. Skolnick, A. V. Gorbach, R. Hartley, D. V Skryabin, E. A. Cerda-Mendez, K. Biermann, R. Hey and P. V. Santos, *Nat. Photon.* 2012, **6**, 50-55.
19. G. La Rocca, *Nat. Photoni.* 2010, **4**, 343-345.
20. D. G. Lidzey, D. D. C. Bradley, M. S. Skolnick, T. Virgili, S. Walker amd D. M. Whittaker, *Nature* 1998, **395**, 53-55.
21. S. Kéna-Cohen and S. R. Forrest, *Nat. Photon.* 2010, **4**, 371-375.
22. K. Takazawa, J. Inoue, K. Mitsuishi and T. Takamasu, *Phys. Rev. Lett.* 2010, **105**, 67401.
23. C. Zhang, C.-L. Zou, Y. Yan, R. Hao, F.-W. Sun, Z.-F. Han, Y. S. Zhao and J. Yao, *J. Am. Chem. Soc.* 2011, **133**, 7276-7279.
24. V. G. Kozlov, V. Bulović, P. E. Burrows and S. R. Forrest, *Nature* 1997, **389**, 362-364.
25. Y. S. Zhao, A. Peng, H. Fu, Y. Ma and J. Yao, *Adv. Mater.* 2008, **20**, 1661-1665.
26. M. Ichikawa, R. Hibino, M. Inoue, T. Haritani, S. Hotta, K. Araki, T. Koyama and Y. Taniguchi, *Adv. Mater.* 2005, **17**, 2073-2077.
27. L. K. van Vugt, B. Piccione and R. Agarwal, *Appl. Phys. Lett.* 2010, **97**, 061115.
28. H. Chen, Y. Weng and J. Zhang, *J. Opt. Soc. Am. B* 2009, **26**, 1627-1634.